Clinical Hemorheology and Microcirculation 69 (2018) 343–354
DOI 10.3233/CH-170275
IOS Press

A two-stage multi-view learning framework based computer-aided diagnosis of liver tumors with contrast enhanced ultrasound images

Le-Hang Guo[a,1], Dan Wang[a,1], Yi-Yi Qian[b], Xiao Zheng[b], Chong-Ke Zhao[a], Xiao-Long Li[a], Xiao-Wan Bo[a], Wen-Wen Yue[a], Qi Zhang[b], Jun Shi[b,*] and Hui-Xiong Xu[a,*]
[a]*Department of Medical Ultrasound, Shanghai Tenth People's Hospital, Ultrasound Research and Education Institute, Tongji University School of Medicine, Shanghai, China*
[b]*Shanghai Institute for Advanced Communication and Data Science, School of Communication and Information Engineering, Shanghai University, Shanghai, China*

Abstract.
OBJECTIVE: With the fast development of artificial intelligence techniques, we proposed a novel two-stage multi-view learning framework for the contrast-enhanced ultrasound (CEUS) based computer-aided diagnosis for liver tumors, which adopted only three typical CEUS images selected from the arterial phase, portal venous phase and late phase.
MATERIALS AND METHODS: In the first stage, the deep canonical correlation analysis (DCCA) was performed on three image pairs between the arterial and portal venous phases, arterial and delayed phases, and portal venous and delayed phases respectively, which then generated total six-view features. While in the second stage, these multi-view features were then fed to a multiple kernel learning (MKL) based classifier to further promote the diagnosis result. Two MKL classification algorithms were evaluated in this MKL-based classification framework. We evaluated proposed DCCA-MKL framework on 93 lesions (47 malignant cancers vs. 46 benign tumors).
RESULTS: The proposed DCCA-MKL framework achieved the mean classification accuracy, sensitivity, specificity, Youden index, false positive rate, and false negative rate of $90.41 \pm 5.80\%$, $93.56 \pm 5.90\%$, $86.89 \pm 9.38\%$, $79.44 \pm 11.83\%$, $13.11 \pm 9.38\%$ and $6.44 \pm 5.90\%$, respectively, by soft margin MKL classifier.
CONCLUSION: The experimental results indicate that the proposed DCCA-MKL framework achieves best performance for discriminating benign liver tumors from malignant liver cancers. Moreover, it is also proved that the three-phase CEUS image based CAD is feasible for liver tumors with the proposed DCCA-MKL framework.

Keywords: Contrast-enhanced ultrasound, artificial intelligence, liver tumor, deep canonical correlation analysis, multiple kernel learning

1. Introduction

Real-time contrast-enhanced ultrasound (CEUS) is now a widely accepted ultrasound imaging technique for diagnosis of liver tumors in clinical practice [1–3]. However, a radiologist usually should conduct a series of complex tasks to provide diagnostic results based on CEUS [4, 5]. Consequently,

[1]These authors contributed equally to this work.

*Corresponding authors: Hui-Xiong Xu, MD, PhD, Department of Medical Ultrasound, Shanghai Tenth People's Hospital, Ultrasound Research and Education Institute, Tongji University School of Medicine, Shanghai 200072, China. E-mail: xuhuixiong@126.com and Jun Shi, PhD, Shanghai Institute for Advanced Communication and Data Science, School of Communication and Information Engineering, Shanghai University, Shanghai, 200444, China.

the radiologist's experience plays a critical role for reliable and accurate diagnosis based on this complex and time-consuming procedure. The complexity of CEUS-based diagnosis has limited the wide application of CEUS to all hospitals, particularly to rural hospitals.

With the fast development of artificial intelligence techniques, the ultrasound-based computer-aided diagnosis (CAD) has shown its effectiveness to work as a second radiologist and then help improve the diagnostic accuracy and the objectivity for various tumor diseases [4, 6–8]. B-mode ultrasound based CAD for liver tumors is one of the most widely investigated topics [9, 10]. More recently, the CEUS-based CAD for liver tumors has attracted considerable attention [4, 11–16]. All these researches indicated the feasibility of CEUS-based CAD for liver tumors, and also showed the potential to expand the application of CEUS in more hospitals.

In clinical practice, the time-intensity curves (TICs) of CEUS represent the perfusion dynamics for different regions as a time function, which correlates with the perfusion kinetics [1]. Therefore, the TICs-based feature extraction algorithms are widely used by considering the lesion perfusion [4,11–16]. However, this kind of feature extraction methods usually suffer from the problems of high computational complexity, because the sequence images in a CEUS video are needed to generate TICs, which is also a time-costing procedure.

It is worth noting that an experienced radiologist can provide reliable and accurate diagnosis about liver tumors mainly only based on several limited and typical CEUS images from three phases in CEUS over time, namely the arterial phase (A-P) (10–30 seconds after contrast administration), portal venous phase (PV-P) (31–120 seconds) and delayed phase (D-P) (121–360 seconds) [1]. Motivated by this diagnosis mode of algorithm radiologists, it is potential to develop a three-phase-image-based CEUS CAD for liver tumor, which only selects three typical CEUS images corresponding to the above-mentioned three enhancement patterns.

Since three images corresponding to the A-P, PV-P and D-P in CEUS represent different properties for liver tumors during the perfusion dynamics procedure, it is natural to take these three CEUS images as multi-view data from the viewpoint of machine learning. Therefore, the multi-view learning (MVL) methods have the potential to perform the feature-level fusion or the classifier- or decision-level fusion for multi-view data in the proposed three-phase-image-based CEUS CAD for liver tumors [17].

The canonical correlation analysis (CCA) is a common used feature-level fusion algorithm with various variants [18], among which the newly proposed deep CCA (DCCA) has achieved superior performance to CCA [19–21]. DCCA simultaneously learns two complex nonlinear mapping of two-view data that are maximally correlated with deep neural networks (DNN) [19]. In the proposed three-phase-image-based CEUS CAD, since three images are selected from the A-P, PV-P and D-P enhancement patterns from the same CEUS procedure, they naturally have correlation between each other. These correlations will benefit the representation of tumor properties in CAD. Therefore, we propose to adopt DCCA to represent the common information between two phases of CEUS images.

On the other hand, when DCCA is applied to three pairs of CEUS images, namely A-P image and PV-P image, A-P image and D-P image, and PV-P image and D-P image, there are totally six-view new features to be generated. The classifier-level fusion then can be adopted to further promote classification performance in CAD. The multiple kernel learning (MKL) is a widely and effectively used classifier-level MVL method for multi-view data, where each kernel naturally corresponds to a feature view [17]. Therefore, the MKL classifier can fuse and classify the learned six-view features by DCCA from three CEUS image pairs, so as to further improve the predictive performance of our proposed CAD.

In this work, we propose a two-stage MVL based framework for CAD of liver tumors with only three CEUS images corresponding to three enhancement patterns. Particularly, DCCA will be conducted on three features pairs among the images of A-P, PV-P and D-P, respectively, and then the generated six-view features are fed to a MKL classifier to predict liver tumors.

2. Material and methods

2.1. Dataset and data preprocessing

The CEUS dataset used in this study was acquired from 93 patients from the university hospital. In this dataset, 47 malignant lesions including 22 hepatocellular carcinomas, 5 cholangiocellular carcinomas and 10 metastatic hepatic carcinomas (metastasized from colorectum) were confirmed by pathological examination with specimens obtained from surgery or biopsy, while the remaining 46 cases were diagnosed with benign by clinical data, patient history, other imaging modalities including CT and MRI (45 haemangiomas), and pathological examination after surgery (1 focal nodular hyperplasia). The approval from the ethics committee of the hospital was obtained (identifier: SHSY-IEC-3.1/16-02/01). The informed consent from the patients was waived due to the retrospective nature of the study.

All CEUS data were sampled from the LOGIQ E9 ultrasound system (GE Healthcare, Milwaukee, WI) with a 1-5M curved-array transducer by an experienced radiologist. Meanwhile, the second-generation contrast agent Sonovue (Bracco, Milan, Italy) was injected intravenously through a cubital vein with the dose of 1.5 ml. The mechanic index was controlled to be less than 0.2 when the contrast-specific mode was applied. Real-time frame-by-frame B-mode and CEUS images were simultaneously recorded as a video file.

The typical three images corresponding to the arterial, portal venous and delayed phases, respectively, were selected by an experienced radiologist. The rectangular ROI in each image was manually extracted by the same radiologist. Figure 1 shows the example ultrasound images of benign liver tumor and malignant liver cancers.

2.2. Two-stage multi-view learning framework

Figure 2 shows the flowchart of the proposed two-stage MVL framework, namely the DCCA-MKL framework, for classification of liver tumors with the A-P image, PV-P image and D-P image.

The detailed steps of DCCA-MKL framework are given as follows:

1) Three typical CEUS images corresponding to the A-P, PV-P and D-P patterns, respectively, are selected from a CEUS video.
2) Features are extracted from the ROI of each liver tumor for each CEUS image.
3) DCCA algorithm is then conducted on three feature pairs between A-P and PV-P images, A-P and D-P images, and PV-P and D-P images, respectively.
4) The generated six-view features in total are finally fed to a MKL-based classifier to provide the predicted diagnosis result of liver tumor. In this framework, we evaluate not only a newly proposed soft margin MKL (SM-MKL) classifier [22], but also the multiple kernel boosting (MKB) algorithms that are another type of MKL classifier [23].

2.3. Extraction of statistical features

Since statistical features can be extracted directly from ROI in images without resizing them to the same size, this kind of feature extraction methods are commonly used in ultrasound images [24]. In this study, we extracted the statistical features from the intensities of all the pixels in ROIs according to reference [24]. These features represented the statistical and texture properties of liver lesions by calculating the mean, standard deviation, skewness, kurtosis, coefficient of variance, entropy of histogram, area ratio, combined area ratio, and several percentiles, etc. In addition, since the gray-level

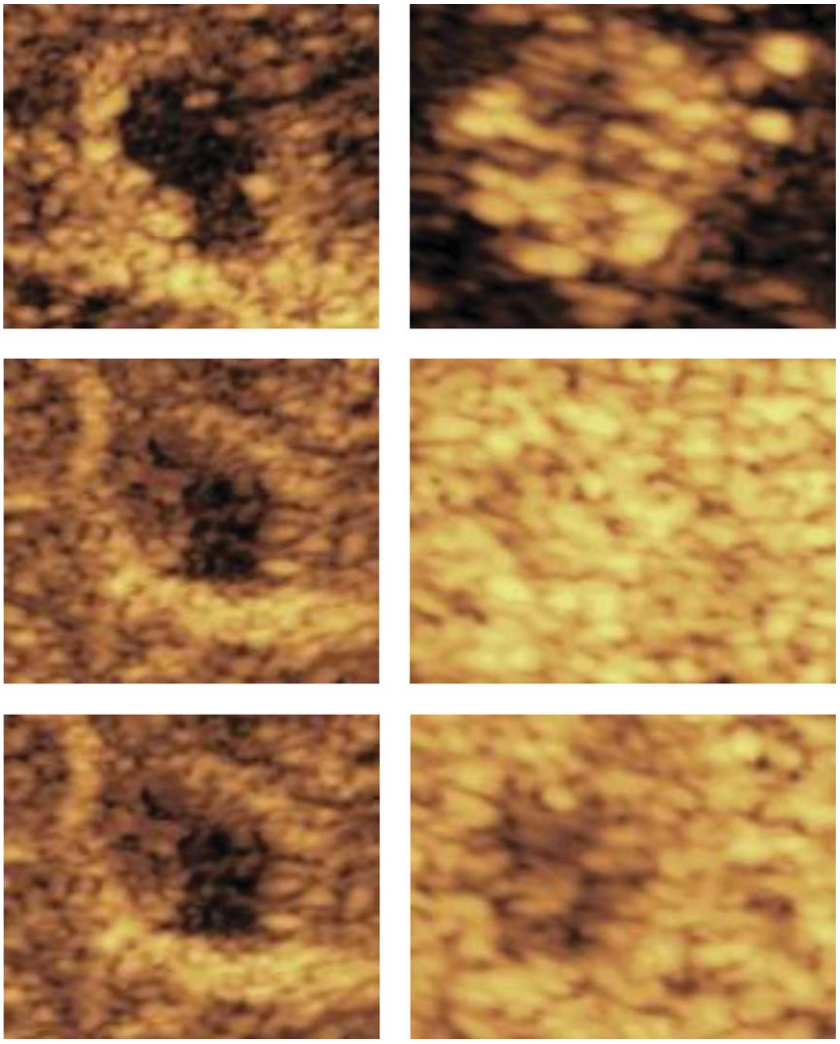

Fig. 1. Example images of benign liver tumor at the left column and malignant liver cancer at the right column with the sequence of arterial phase image, portal phase image and delayed phase image from top to bottom.

co-occurrence matrix (GLCM) is very commonly used for texture feature extraction, other statistical texture features were calculated from it, including the energy, contrast, homogeneity and entropy of GLCM. Finally, totally 66-dimensional features were extracted for each CEUS image.

2.4. Deep canonical correlation analysis

A fast DCCA algorithm is adopted in this work [19, 20], whose structure is shown in Fig. 3.

Let X_1 and X_2 denote two feature sets corresponding to the two features among A-P image, PV-P image and D-P image sets, and $x_{1i} \in X_1$ and $x_{2i} \in X_2$ be the samples with the feature dimensionality of d_1 and d_2, respectively. Define f and g as two features mappings for View-1 and View-2, respectively. The objective of the original CCA is to find $L \leq \min(d_1, d_2)$ pairs of linear projection vectors U and V, such that the projections of each view is maximally correlated with their counterparts in the other view. The objective function is given by

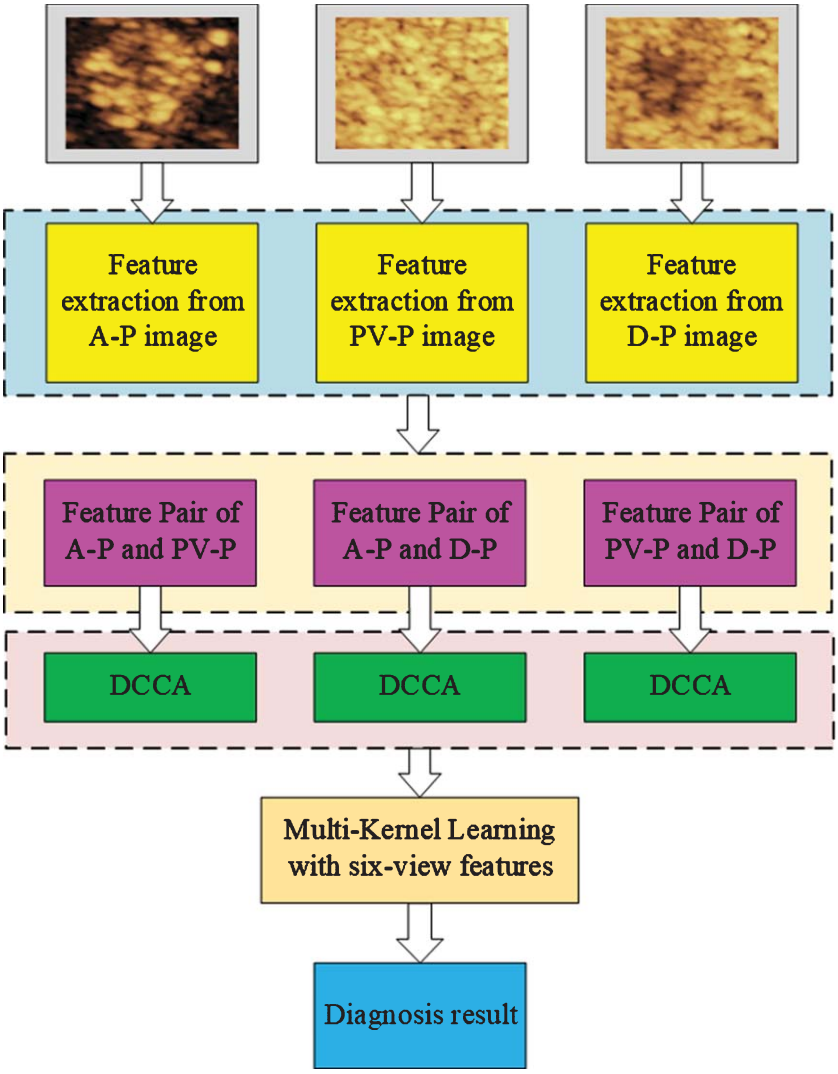

Fig. 2. Flowchart of the DCCA-MKL framework for classification of liver tumors.

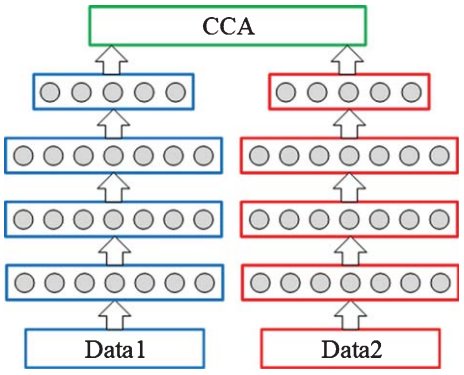

Fig. 3. Schematic diagram of deep canonical correlation analysis.

$$\begin{aligned} &max_{U,V}\left(\tfrac{1}{N}tr\left(U^T F G^T V\right)\right) \\ &s.t.\, U^T\left(\tfrac{FF^T}{N}+r_{X1}I\right)U = V^T\left(\tfrac{GG^T}{N}+r_{X2}I\right)V = I \end{aligned} \tag{1}$$

where $F = f(X_1)$ and $FG = g(X_1)$, r_{X1} and r_{X2} are regularization parameters.

As shown in Fig. 2, DCCA learns the complex nonlinear representations of two-view data with DNN. Specially, f and g are two DNNs in DCCA, and their output layers are maximally correlated by CCA.

For dataset 1, the outputs of the j-th layer in the K-layer deep networks is given by

$$f_j(x_{1i}) = s\left(W_j^f x_{1i} + b_j^f\right) \tag{2}$$

where W_i^f is the matrix of weights, b_j^f is the vector of biases, and s is a nonlinear function applied componentwise. The output f_j is used as the input for the next (j+1) layer network. A K-layer neural network implements the nested mapping $f(X_1)$.

For dataset 2, the representation $g(X_2)$ is calculated in the same way with different parameters W_j^g and b_j^g.

The goal of DCCA is to jointly learn the parameters for both views W^f, W^g, b^f and b^g, such that the corr $(f(X_1),\ g(X_2))$is as high as possible. This problem can be solved by:

$$min_{W_f,W_g,U,V}\left(-\frac{1}{N}tr\left(U^T F\left(X_1;W_f\right)G\left(X_2;W_g\right)^T V\right)\right) \tag{3}$$

where the constrain of Equation (3) is the same as that in Equation (1). A fast stochastic optimization for Equation (3) is proposed in [20].

The final DCCA features (projections) are $\tilde{f}(x_{1i}) = U^T f(x_{1i})$ for dataset 1 and $\tilde{g}(x_{2i}) = U^T g(x_{2i})$ for dataset 2. Therefore, there were totally six-view new features generated in this work.

Please refer to [19] and [20] for more information about DCCA.

2.5. Multiple kernel learning

We propose a two-stage MVL based framework for CEUS-based CAD to diagnosis liver tumors. In this framework, the MKL-based classifier can be flexibly used due to the diverse of MKL algorithms. In this work, the SM-MKL algorithm and MKB algorithm are selected as a classifier, respectively, to evaluate the effectiveness of the proposed DCCA-MKL framework.

For kernel algorithms, such as support vector machines (SVM), the solution for the learning problem is written as [17]:

$$h(x) = \sum\nolimits_{i=0}^{l} \alpha_i k(x, x_i) + b \tag{4}$$

where x_i is the training sample, α_i and b are the coefficients to be learned from training samples, and $k(x, x_i)$ is a given positive definite kernel associated with a reproducing kernel Hilbert space (RKHS).

MKL aims to learn an optimal combination of multiple kernels usually given by

$$k(x, x_i) = \sum\nolimits_{i=0}^{m} \beta_i k_i(x, x) \tag{5}$$

where m is the total number of kernels, and β_i is the weight for each basis kernel.

2.5.1. Soft margin MKL algorithm

MKL should learn both coefficients and weights in a single optimization problem. Various optimization methods have been proposed to solve the kernel combination problem. The recently proposed soft

margin MKL (SM-MKL) algorithm was first selected as the classifier due to its effectiveness [22]. SM-MKL is in analogy to the well-known soft margin SVM by introducing an additional slack variable called kernel slack variable for each quadratic constraint of MKL. Moreover, a new block-wise coordinate descent algorithm is proposed to efficiently solve the new hinge loss SM-MKL problem. SM-MKL is therefore more robust for real applications.

The hinge loss is used for the kernel slack variables in this work [22]. The objective function for the hinge loss SM-MKL is given by

$$\min \tau, \alpha, \in, A, \zeta_m - \tau + \theta \sum\nolimits_{\mathrm{m}=1}^{\mathrm{M}} \zeta_{\mathrm{m}} s.t.\ \mathrm{SVM}\{\mathrm{K}_m, \alpha\} \geq \tau - \zeta_m,\ \zeta_m \geq 0,\ m = 1, \ldots, M. \quad (6)$$

where τ is the margin, ζ_m is the m-th slack variable corresponding to the m-th kernel, and θ balances the contribution of the loss term represented by slack variables and margin. The objective of Equation (6) was to maximize the margin while considering the "errors" from the given M base kernels at the same time. The block-wise coordinate descent algorithm is then proposed as the optimization for SM-MKL.

More detailed introduction about SM-MKL is referred to [22].

2.5.2. Multiple kernel boosting algorithm

MKB is another kind of MKL method, which converts the standard MKL formulation to a linear combination of the real outputs of multiple single-kernel SVM classifiers [23]. Here we rewrited the decision function as

$$Y(x) = \sum\nolimits_{i=1}^{n} \beta_i \sum\nolimits_{l}^{m} \mu_i y_i k_l(x, x_i) + \tilde{b} = \sum\nolimits_{l}^{M} \beta_l \left(\mu^{\mathrm{T}} \mathbf{K}_l(x) + \tilde{b}_l\right) \quad (7)$$

where μ_i is the Lagrange multiplier, $\mathbf{K}_l(x) = [k_l(x, x_1), k_l(x, x_2), \ldots, k_l(x, x_N)]^T$ and $\tilde{b} = \sum_{l=1}^{M} \tilde{b}_l$.

In [23], the boosting algorithm was used instead of the simple combination of single-kernel SVMs in the MKL method, to avoid solving a complex optimization problem for computing $\{\beta_l\}_1^L$. By setting the decision function of a single-kernel SVM as

$$h_l(x) = \mu^{\mathrm{T}} \mathbf{K}_l(x) + \tilde{b}_l \quad (8)$$

Equation (&) can be written as

$$Y(x) = \sum\nolimits_{j=1}^{J} \beta_j h_j(x) \quad (9)$$

where J denotes the number of iterations in the boosting process, and here the notation l is replaced by j to indicate the index of iteration rather than the kernel function. Equation (9) means that each SVM is considered as a weak classifier, and the final strong classifier $Y(x)$ is the weighted combination of all the weak classifiers.

The weighted classification error of a single SVM+ classifier at the j-th iteration was defined as

$$\varepsilon_j = \frac{\sum_{i=1}^{N} \omega(i) |h_j(x_i)| \left(\mathrm{sign}\left(-y_i h_j(x_i)\right) + 1\right)/2}{\sum_{i=1}^{N} \omega(i) |h_j(x_i)|} \quad (10)$$

where $\omega(i)$ is the weight of the training samples. The combination coefficient β_j is calculated by

$$\beta_j = \frac{1}{2} \log \frac{1 - \varepsilon_l}{\varepsilon_l} \cdot \frac{1}{2} \left(sign\left(\log \frac{1 - \varepsilon_l}{\varepsilon_l}\right) + 1\right) \quad (11)$$

In addition, the weight was updated by the following equation

$$w_{j+1}(i) = \frac{w_j(i)\, e^{-\beta_j l_j h_j(x_i)}}{2\sqrt{\varepsilon_l(\varepsilon_l - 1)}} \quad (12)$$

After J iterations, all the β_j and $h_j(x_i)$ were calculated and the final boosted classifier is achieved.

2.6. Experiment

Our experiments mainly evaluated the performance of DCCA-MKL framework. Since DCCA-MKL framework mainly includes two components, namely DCCA and MKL, DCCA was compared with the traditional CCA algorithm performed on pairs of CEUS images, and both SM-MKL and MKL algorithms were compared with the most commonly used majority-voting-based multi-view ensemble learning algorithm.

The proposed DCCA-MKL framework was first compared with the following single-view feature based classification: (1) the statistical features extracted from the CEUS image of A-P; (2) the statistical features extracted from the CEUS image of PV-P; (3) the statistical features extracted from the CEUS image of D-P. The SVM classifier with linear kernel was used for all single-view features.

Moreover, DCCA-MKL framework was also compared with the following multi-view feature based algorithms: (4) the voting-based classification algorithm for the six-view features generated by CCA (CCA-Voting); (5) SM-MKL algorithm conducted on the six-view features generated by CCA (CCA-MKL); (6) MKB algorithm conducted on the six-view features generated by CCA (CCA-MKB); (7) the voting-based classification algorithm for the six-view features by DCCA(DCCA-Voting); (8) SM-MKL algorithm conducted on the six-view features generated by DCCA (DCCA-MKL); (9) MKB algorithm conducted on the six-view features generated by DCCA (DCCA-MKB).

The 5-fold cross-validation strategy was performed on all algorithms to avoid the sampling bias introduced by randomly partitioning dataset in the cross-validation. The classification accuracy, sensitivity, specificity, Youden index, false positive rate and false negative rate were used as evaluation indices. Moreover, the receiver operating characteristic (ROC) curve and the area (AUC) under ROC curve were also used as evaluation indices. The classification result was given by the format of mean $\pm$ SD (standard deviation) over repeated runs.

3. Results

Table 1 shows the classification results of different algorithms. It was found that the DCCA-MKL with SM-MKL algorithm achieved the best mean classification accuracy, sensitivity and FNR of $90.41 \pm 5.80\%$, $93.56 \pm 5.90\%$ and $6.44 \pm 5.90\%$, respectively, improved by at least 0.99%, 2.00% and 1.56% compared with all other algorithms in terms of accuracy and sensitivity, respectively. DCCA-MKL also gets the second-best specificity of $86.89 \pm 9.38\%$. DCCA-MKB gets the best Youden index of $80.89 \pm 16.17\%$, and the second-best accuracy of $90.41 \pm 7.83\%$ and specificity of $89.11 \pm 13.62\%$. Other results of DCCA-MKB are also close to those of DCCA-MKL.

Moreover, DCCA-based algorithms (DCCA-Voting, DCCA-MKB and DCCA-MKL) are superior to the corresponding CCA-based algorithms, respectively. Specifically, DCCA-MKL achieves 3.39%, 2.00%, 4.67%, 11.88%, 4.67% and 2.00% improvements over CCA-MKL, on classification accuracy, sensitivity, specificity, Youden index, FPR and FNR, respectively; while DCCA-MKB improves 4.33%, 8.89%, 8.67%, 8.89% and compares with CCA-MKB on classification accuracy, specificity, Youden index, and FPR, respectively. The results indicate that DCCA can effectively fuse and represent multi-view features for CEUS images, and both SM-MKL and MKB further promoted classification performance.

Figure 4 shows the ROC curves, and the corresponding AUC values are shown in Table 2. It can be found that the proposed DCCA-MKB algorithm again gets the best AUC value of 0.974, and DCCA-MKL is next to it with the AUC value of 0.953.

Table 1
Classification results of different algorithms (UNIT: %)

Algorithm	Accuracy	Sensitivity	Specificity	Youden index	False positive rate	False negative rate
A-P-SVM	73.10 ± 9.88	83.11 ± 18.37	62.89 ± 23.25	45.00 ± 19.85	37.11 ± 23.25	16.89 ± 18.37
PV-P-SVM	84.85 ± 7.40	89.56 ± 10.59	80.44 ± 21.34	68.56 ± 18.58	19.56 ± 21.34	10.44 ± 10.59
D-P-SVM	72.11 ± 6.80	66.44 ± 24.75	77.78 ± 28.33	72.22 ± 27.46	22.22 ± 28.33	33.56 ± 24.75
CCA-Voting	86.02 ± 8.82	85.56 ± 13.70	86.67 ± 9.30	65.78 ± 7.13	13.33 ± 9.30	14.44±13.70
CCA-MKB	86.08 ± 7.97	92.00 ± 10.95	80.22 ± 9.60	72.22 ± 16.14	19.78 ± 9.60	8.00 ± 10.95
CCA-MKL	87.02 ± 7.27	91.56 ± 9.18	82.22 ± 12.67	67.56 ± 10.58	17.78 ± 12.67	8.44 ± 9.18
DCCA-Voting	89.42 ± 9.81	89.78 ± 10.01	**89.33 ± 15.35**	72.22 ± 27.46	**10.67 ± 15.35**	10.22 ± 10.01
DCCA-MKB	90.41 ± 7.83	91.78 ± 8.45	89.11 ± 13.62	**80.89 ± 16.17**	10.89 ± 13.62	8.22 ± 8.45
DCCA-MKL	**90.41 ± 5.80**	**93.56 ± 5.90**	86.89 ± 9.38	79.44 ± 11.83	13.11 ± 9.38	**6.44 ± 5.90**

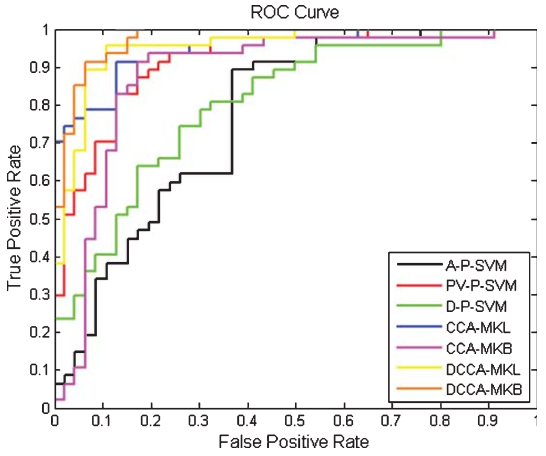

Fig. 4. ROC curves of different algorithms.

Table 2
AUC Values of different algorithms

Algorithm	AUC	Algorithm	AUC
A-P-SVM	0.768	CCA-MKL	0.950
PV-P-SVM	0.917	CCA-MKB	0.877
D-P-SVM	0.803	DCCA-MKL	0.953
		DCCA-MKB	**0.974**

AUC: Area under ROC curve.

4. Discussion

In this work, a new CEUS-based CAD system for liver tumor is developed. The main contributions of this work are twofold: (1) Motivated by the CEUS-based clinical diagnosis mode of radiologists that only adopts several images from three typical CEUS phases for liver tumors, we proposed a three-phase-image-based CEUS CAD for liver tumors with the advantages of low computational complexity but together with high diagnosis accuracy; (2) We further developed a two-stage MVL

framework by integrating DCCA and MKL algorithms (DCCA-MKL in short) to effectively fuse the feature representation of three-phase CEUS images and then discriminating benign liver tumors from malignant liver cancers. The experimental results on 93 patients show the effectiveness of the developed DCCA-MKL framework.

This proposed DCCA-MKL framework performs both feature-level and classifier-level MVL in an integrated framework to achieve superior classification results. Since there are correlations among three-phase CEUS images, it is natural to explore these relationships to promote feature representation for classification. Therefore, we adopt DCCA (or CCA) algorithm as the feature-level MVL algorithm to extract and fuse the correlations among three pairs of three-phase images in the first stage. The experimental results in Table 1 show the effectiveness of both DCCA and CCA, because all the DCCA- and CCA-based algorithms outperform the single-phase-image-based algorithm. Moreover, DCCA achieves superior performance to CCA, because the DNN component in DCCA effectively improved the feature representation performance of the original features by hierarchically learning higher-level features, while CCA only directly conducts on the original features.

On the other hand, the multi-view features generated DCCA have not only the individual information of three phases, but also the correlated information among them. The simplest way to fuse these multi-view features is to concatenate all the six-view features to form a vector. However, some properties in different views will generally be essentially lost, resulting in depressed feature representation. Therefore, we apply MKL algorithm to fuse these features and perform classification simultaneously in the second stage. The results indicate that MKL-based algorithms further promote classification performance. Furthermore, different view features have different powers of feature representation, resulting in different impacts on final classifier. Different from the voting-based ensemble learning algorithm that supposes different view features with same impacts and given the same weights to the classifiers corresponding to different views, MKL methods then give different weights to different view features. As a consequence, both MKB and SM-MKL algorithms outperform the voting-based ensemble classifier.

It is worth noting that to the best of our knowledge, both DCCA and CCA have not been applied to represent features and explore correlations for CEUS images, because the features were mainly directly extracted from TICs of whole CEUS videos in previous work [4, 11–16]. Although in [11] and [15], additional morphologic and texture features were extracted from CEUS images, they employed Microflow imaging technique to obtain images with accumulated inflow signals after bursting microbubbles for further analysis. On the contrast, we proposed to analyze three images directly from three enhanced phases based on real-time inflow signals without any burst scans. In [16], Kondo et al. proposed to extract spatial and temporal features in the arterial, portal and postvascular phases as well as max-hold images with perflubutane microbubbles; however, these features were still mainly extracted based on TICs. The DCCA-MKL framework only extracted features from three images corresponding to three enhanced phases without extracting TICs, and therefore it had low computational complexity. On the other hand, Wu et al. employ the deep belief networks (DBN) to simultaneously learn feature representation from the TICs-based features and perform classification task of liver disease [13]. Although DCCA is also a deep learning algorithm, it mainly learns new feature representation and explore the correlated information from two-view data [19, 20], which is different from DBN. Moreover, MKL methods are also seldom used for CEUS-based CAD system as classifier.

The proposed two-stage MVL framework is very flexible for application, because different MVL algorithms can be easily adopted in it. For example, SM-MKL and MKB are two different kinds of MKL algorithms, and both have been evaluated in this framework with excellent classification results in current work. Moreover, other feature-level multi-modal fusion algorithms can be used to fuse and learning feature representation instead of DCCA for multi-view CEUS images.

At present, there are two primary limitations with this study. First, the sample size was relative small. Therefore, further study on a larger group of patients is required. On the other hand, the three images for analysis are manually selected. As a result, the representation of the selected image may be significantly influenced by human factors.

In future work, other multi-modal feature fusion algorithms, such as multi-modal deep neural networks algorithm [25], will be adopted instead of DCCA to more effectively fuse and learn feature representation of three-phase CEUS images. Of course, other classifier-level MVL algorithms also should be evaluated in future. Moreover, we will study the methods of automatically identifying and selecting the optimal images corresponding to the arterial, portal venous and delayed phases, and then implement the automatic CAD system for liver lesions. On the other hand, the B-mode ultrasound imaging is routinely used for the detection and diagnosis of liver lesions, and provides different diagnosis information compared to CEUS images. Therefore, B-mode ultrasound image can be integrated into the current three phase CEUS image based CAD system to further promote the predictive performance.

5. Conclusion

In conclusion, we propose a two-stage MVL framework, namely DCCA-MKL framework, for three-phase-image-based CEUS CAD for liver tumors. The experimental results show that DCCA can effectively learn the correlations among three-phase images, while both SM-MKL and MKB algorithms can further promote classification performance. Therefore, the proposed DCCA-MKL framework has high prediction performance while with low computational complexity. It suggests that the DCCA-MKL framework has the potential for CEUS-based CAD for liver tumors.

Acknowledgments

This work is supported by the grants from Shanghai Health Bureau (20114003 and 2013SY066), Shanghai Hospital Development Center (12014229, 22015005 and 16CR3061B), Science and Technology Commission of Shanghai Municipality (14441900900), and the National Natural Science Foundation of China (81371570, 61471231, 81627804, 81671695, 61401267, 61671281).

References

[1] Claudon M, Dietrich CF, Choi BI, et al. Guidelines and good clinical practice recommendations for contrast enhanced ultrasound (CEUS) - update 2008. Ultrasound Med Biol. 2008;29:28-44.

[2] Haimerl M, Poelsterl S, Beyer LP, Wiesinger I, Nießen C, Stroszczynski C, Wiggermann P, Jung EM. Chronic liver disease: Quantitative MRI vs CEUS-based microperfusion. Clin Hemorheol Microcirc. 2016;64:435-46.

[3] Schellhaas B, Waldner MJ, Görtz RS, et al. Diagnostic accuracy and interobserver variability of Dynamic Vascular Pattern (DVP) in primary liver malignancies - A simple semiquantitative tool for the analysis of contrast enhancement patterns. Clin Hemorheol Microcirc. 2017;66:317-31.

[4] Bakas S, Makris D, Sidhu PS, Chatzimichail K. Automatic identification and localisation of potential malignancies in contrast-enhanced ultrasound liver scans using spatio-temporal features. The 6th Int. Workshop Abdominal Imaging Computational and Clinical Applications. 2015:13-22.

[5] Jung EM, Clevert DC, Schreyer AG, et al. Evaluation of quantitative contrast harmonic imaging to assess malignancy of liver tumors: A prospective controlled two-center study. World J Gastroenterol. 2007;13:6356-64.

[6] Zhou SC, Shi J, Zhu J, Cai Y, Wang RL. Shearlet-based texture feature extraction for classification of breast tumor in ultrasound image. Biomed Signal Proces. 2013;8(6):688-96.

[7] Huang QH, Yang FB, Liu LZ, Li XL. Automatic segmentation of Breast lesions for interaction in ultrasonic computer-aided diagnosis. Inform Sciences. 2015;314:293-310.
[8] Shi J, Zhou S, Liu X, Zhang Q, Lu M, Wang T. Stacked deep polynomial network based representation learning for tumor classification with small ultrasound image dataset. Neurocomputing. 2016;194:87-94.
[9] Acharya UR, Faust O, Molinari F, Sree SV, Junnarkar SP, Sudarshan V. Ultrasound-based tissue characterization and classification of fatty liver disease: A screening and diagnostic paradigm. Knowl-Based Syst. 2015;75:66-77.
[10] Bharti P, Mittal D, Ananthasivan R. Computer-aided characterization and diagnosis of diffuse liver diseases based on ultrasound imaging: A review. Ultrasonic Imaging. 2017;39:33-61.
[11] Shiraishi J, Sugimoto K, Moriyasu F, Kamiyama N, Doi K. Computer-aided diagnosis for the classification of focal liver lesions by use of contrast-enhanced ultrasonography. Med Phys. 2008;35:1734-46.
[12] Streba CT, Ionescu M, Gheonea DI, Sandulescu L, Ciurea T, Saftoiu A, Vere CC, Rogoveanu I. Contrast-enhanced ultrasonography parameters in neural network diagnosis of liver tumors. World J Gastroenterology. 2012;18:4427-34.
[13] Wu K, Chen X, Ding M. Deep learning based classification of focal liver lesions with contrast-enhanced ultrasound. Optik - Int J Light Electron Opt. 2014;125:4057-63.
[14] Gatos I, Tsantis S, Spiliopoulos S, Skouroliakou A, Theotokas I, Zoumpoulis P, Hazle JD, Kagadis GC. A new automated quantification algorithm for the detection and evaluation of focal liver lesions with contrast-enhanced ultrasound. Med Phys. 2015;42:3948-59.
[15] Sugimoto K. Shiraishi J, Tanaka H, Tsuchiya K, Aso K, Kobayashi Y, Iijima H, Moriyasu F. Computer-aided diagnosis for estimating the malignancy grade of hepatocellular carcinoma using contrast-enhanced ultrasound: An ROC observer study. Liver Int. 2016;36:1026-1032.
[16] Kondo S, Takagi K, Nishida M, Iwai T, Kudo Y, Ogawa K, Kamiyama T, Shibuya H, Kahata K, Shimizu C. Computer-aided diagnosis of focal liver lesions using contrast-enhanced ultrasonography with perflubutane microbubbles. IEEE Trans Med Imaging. 2017.
[17] Xu C, Tao D, Xu C. A survey on multi-view learning. arXiv. 2013:1304.5634.
[18] Hotelling H. Relations between two sets of variates. Biometrika. 1936;28:321-377.
[19] Andrew G, Arora R, Bilmes J. Livescu K. Deep canonical correlation analysis. The 30th International Conference on Machine Learning. 2013:1247-55.
[20] Wang W, Arora R, Livescu K, Bilmes JA. Unsupervised learning of acoustic features via deep canonical correlation analysis, IEEE International Conference on Acoustics. Speech and Signal Processing. 2015:4590-4.
[21] Shao J, Wang L, Zhao Z, Su F, Cai A. Deep canonical correlation analysis with progressive and hypergraph learning for cross-modal retrieval. Neurocomputing. 2016;214:618-28.
[22] Xu X, Tsang IW, Xu D. Soft margin multiple kernel learning. IEEE Trans Neural Network Learn Sys. 2013;24:749-61.
[23] Yang F, Lu H, Yang M. Robust visual tracking via multiple kernel boosting with affinity constraints. IEEE Trans Circuits Syst Video Technol. 2014;24:242-54.
[24] Zhang Q, Xiao Y, Suo J, Shi J, Yu J, Guo Y, Wang Y, Zheng H. Sonoelastomics for breast tumor classification: A radiomics approach with clustering-based feature selection on sonoelastography. Ultrasound Med Biol. 2017.
[25] Shi J, Zheng X, Ying SH, Zhang Q, Li Y. Multimodal neuroimaging feature learning with multimodal stacked deep polynomial networks for diagnosis of Alzheimer's disease. IEEE J Biomed Health Inform. 2017.